First-principles study of native defects and lanthanum impurities in NaTaO3

AUTHOR(S):

Choi, Minseok; Oba, Fumiyasu; Tanaka, Isao

CITATION:

Choi, Minseok ...[et al]. First-principles study of native defects and lanthanum impurities in NaTaO3. PHYSICAL REVIEW B 2008, 78(1): 014115.

ISSUE DATE:

2008-07

URL:

http://hdl.handle.net/2433/84634

PHYSICAL REVIEW B **78**, 014115 (2008)

First-principles study of native defects and lanthanum impurities in $NaTaO_3$

Minseok Choi,[1] Fumiyasu Oba,[1,*] and Isao Tanaka[1,2]
[1]*Department of Materials Science and Engineering, Kyoto University, Sakyo, Kyoto 606-8501, Japan*
[2]*Nanostructures Research Laboratory, Japan Fine Ceramics Center, Atsuta, Nagoya 456-8587, Japan*
(Received 30 April 2008; revised manuscript received 26 June 2008; published 30 July 2008)

The formation energies and electronic structure of lattice vacancies, antisite defects, and lanthanum impurities in $NaTaO_3$ are investigated using first-principles calculations based on density-functional theory. The Na antisite and the Ta vacancy, which are both multiple acceptors, are energetically favorable under O-rich conditions, whereas the O vacancy, which is a double donor, is preferred under O-poor conditions. The Ta antisite is a quadruple donor but its high formation energy renders it unlikely to be stable under the thermal equilibrium other than *p*-type and O-poor conditions. In La-doped $NaTaO_3$, substitutional La at the Na site is likely to form as a double donor under O-poor conditions. It is expected to generate carrier electrons except for heavily doped cases where compensation by acceptorlike La at the Ta site, as well as the native acceptors, is significant. For all the native defects and La impurities, no localized one-electron states are found in the band gap, which is consistent with the shallow donor/acceptor behavior determined using the formation energies.

DOI: 10.1103/PhysRevB.78.014115 PACS number(s): 61.72.J−, 61.72.S−, 71.55.Ht

I. INTRODUCTION

In recent years, the photocatalytic water splitting into H_2 and O_2 has been extensively studied because of its great possibility as a source of clean and renewable hydrogen energy.[1] To date, numerous photocatalytic materials have been found, e.g., TiO_2 (Refs. 2–4), $SrTiO_3$ (Refs. 5 and 6), $K_4Nb_6O_{17}$ (Ref. 7), $Sr_2Nb_2O_7$ (Refs. 8 and 9), Ta_2O_5 (Ref. 10), and $NaTaO_3$ (Refs. 11–14). Among them, perovskite-type $NaTaO_3$ is a candidate for a high-efficiency photocatalyst. This material shows promising stability and high photocatalytic activity under ultraviolet light irradiation ($\lambda < 300$ nm) (Refs. 11–14). In particular, La-doped $NaTaO_3$ with loaded NiO has been reported to show very high photocatalytic efficiency for water splitting giving a 56% quantum yield at $\lambda = 270$ nm (Ref. 11).

For high photocatalytic activity, certain physical and chemical properties are required: (i) *a high concentration of charge carriers*—a large number of photogenerated electrons and holes and their separation are important for improving the catalytic activity; (ii) *large surface area*—this can affect the number of sites where photocatalytic activation takes place; and (iii) *good crystallinity and purity*—since native point defects and impurities, as well as line and planar defects, can act as recombination centers of the photogenerated electrons and holes, their concentrations should be reduced. For further development of highly efficient photocatalysts, therefore, a systematic study of the defect properties of candidate materials is necessary. In the case of TiO_2, a prototypical photocatalyst that is commercially used, the behavior of native defects and various impurities in the bulk and on the surface has been intensively studied both theoretically and experimentally.[15–17] On the other hand, the defect properties in $NaTaO_3$ are not well explored theoretically in particular. The understanding in the mechanism of how La doping leads to the observed photocatalytic efficiency, which can be related to the change in carrier concentration,[11] is also limited.

In this work, we present a comprehensive study on the native defects and lanthanum impurities in $NaTaO_3$. Our aim is to elucidate: (i) which native defects are likely to form; (ii) which atomic site is preferable for doped La; and (iii) how native defects and doped La affect the carrier concentration in $NaTaO_3$:La. Through the first-principles calculations of the defect formation energies and electronic structure, we address these issues here.

II. METHODOLOGY

A. Formation energy and transition level

The formation energy of a defect or impurity is estimated as[18]

$$E^f(D,q) = E_T(D,q) - E_T(\text{perfect}) - \sum_i n_i\mu_i + q(E_{\text{VBM}} + E_F), \tag{1}$$

where $E_T(D,q)$ is the total energy of a supercell with one defect or impurity D in charge state q and E_T(perfect) is the total energy of the perfect-crystal supercell. n_i is the number of atoms of type i being added to ($n_i > 0$) and/or removed from ($n_i < 0$) in the perfect-crystal supercell and μ_i is the atomic chemical potential. E_{VBM} is the energy of the valence-band maximum (VBM) and E_F is the Fermi level measured from the VBM, varying in the range of the band gap E_g. The defect transition level $\varepsilon(q/q')$ is described by the Fermi level where the formation energy for charge state q equals that for another charge state q',

$$\varepsilon(q/q') = [E^f_{\text{VBM}}(D,q) - E^f_{\text{VBM}}(D,q')]/(q' - q), \tag{2}$$

where $E^f_{\text{VBM}}(D,q)$ is the defect formation energy for charge state q when E_F is at the VBM.

In compound systems, the defect formation energy depends on the atomic chemical potential μ_i. For ternary $NaTaO_3$, the limit of μ_i (i=Na, Ta, and O) is determined from the equilibrium conditions with various phases containing Na, Ta, and O. The chemical potentials of the three elements should be correlated as

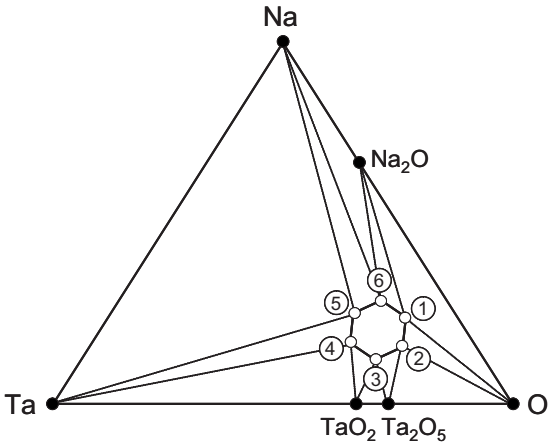

FIG. 1. Schematic phase diagram of the Na-Ta-O ternary system.

$$\mu_{\mathrm{Na}} + \mu_{\mathrm{Ta}} + 3\mu_{\mathrm{O}} = \mu_{\mathrm{NaTaO_3(bulk)}}, \tag{3}$$

where $\mu_{\mathrm{NaTaO_3(bulk)}}$ is the chemical potential of the $NaTaO_3$ perfect crystal. Figure 1 shows a schematic phase diagram of the Na-Ta-O ternary system. The six conditions (1–6) indicated in the diagram correspond to the vertices of the single phase region where equilibrium conditions are given in addition to Eq. (3) as

$$\text{condition } 1{:}\, 2\mu_{\mathrm{Na}} + \mu_{\mathrm{O}} = \mu_{\mathrm{Na_2O(bulk)}}, \quad \mu_{\mathrm{O}} = \frac{1}{2}\mu_{\mathrm{O_2(molecule)}}, \tag{4}$$

$$\text{condition } 2{:}\, \mu_{\mathrm{O}} = \frac{1}{2}\mu_{\mathrm{O_2(molecule)}}, \quad 2\mu_{\mathrm{Ta}} + 5\mu_{\mathrm{O}} = \mu_{\mathrm{Ta_2O_5(bulk)}}, \tag{5}$$

$$\text{condition } 3{:}\, 2\mu_{\mathrm{Ta}} + 5\mu_{\mathrm{O}} = \mu_{\mathrm{Ta_2O_5(bulk)}}, \tag{6}$$

$$\mu_{\mathrm{Ta}} + 2\mu_{\mathrm{O}} = \mu_{\mathrm{TaO_2(bulk)}},$$

$$\text{condition } 4{:}\, \mu_{\mathrm{Ta}} + 2\mu_{\mathrm{O}} = \mu_{\mathrm{TaO_2(bulk)}}, \tag{7}$$

$$\mu_{\mathrm{Ta}} = \mu_{\mathrm{Ta(bulk)}},$$

$$\text{condition } 5{:}\, \mu_{\mathrm{Ta}} = \mu_{\mathrm{Ta(bulk)}}, \quad \mu_{\mathrm{Na}} = \mu_{\mathrm{Na(bulk)}}, \tag{8}$$

$$\text{condition } 6{:}\, \mu_{\mathrm{Na}} = \mu_{\mathrm{Na(bulk)}}, \quad 2\mu_{\mathrm{Na}} + \mu_{\mathrm{O}} = \mu_{\mathrm{Na_2O(bulk)}}. \tag{9}$$

For the chemical potentials of the reference phases, the calculated total energies of the Na (Im $\bar{3}m$), Ta (Im $\bar{3}m$), Na_2O (Fm $\bar{3}m$), TaO_2 ($P4_2/mnm$), and Ta_2O_5 ($Pcmm$) crystals and the O_2 molecule, as well as that of the $NaTaO_3$ perfect crystal, were used. For La impurities, we assumed that the solubility limit was determined by an equilibrium with La_2O_3 ($P\bar{3}m1$). Thus, the value of μ_{La} depends on that of μ_{O} through the relation $2\mu_{\mathrm{La}}+3\mu_{\mathrm{O}}=\mu_{\mathrm{La_2O_3(bulk)}}$.

The calculated formation energy can include some systematic errors due to the approximation to the density-functional theory and the limitation in the simulation cell for defects. Therefore, we should consider some reasonable corrections:

(i) *VBM alignment*—E_{VBM} in defective supercells is generally different from E_{VBM} in a perfect-crystal supercell, and this difference becomes large when supercells contain highly charged defects.[18] Thus, it is necessary to line up E_{VBM} between the perfect and defective supercells. For this purpose, average potentials in a perfect-crystal supercell and those in a bulklike environment far from the defects in defective supercells were used as references.[19–23]

(ii) *Band-gap correction*—the underestimation of E_g caused by the generalized gradient approximation (GGA) employed in the present calculations can be reflected in the defect formation energies. To correct such GGA band-gap error, the energy of the conduction-band minimum (CBM) E_{CBM} was simply increased to agree with the experimental band gap. Following the shift of E_{CBM}, the formation energies of defects with electronic states showing conduction-bandlike characteristics were raised by adding $m\Delta E_g$, where m is the number of electrons at the defect state and ΔE_g is the difference between the experimental and calculated band gaps.[24]

(iii) *Image charge interaction correction*—the Makov-Payne[25] method is often employed for the correction of electrostatic interactions between the image charges generated by charged defects in semiconductors and insulators. It models the interactions with a multipole expansion leading to L^{-1}, L^{-3}, and L^{-5}-dependent terms where L denotes inter-defect distance. The formal charges of defects are used for the L^{-1} term describing the monopole-monopole interactions, i.e., Madelung energies.[26] However, the use of formal charges can overestimate or underestimate the correction of the Madelung energies depending on the spatial distribution of the defect-induced charge density.[18,27–29] In addition, for systems where elastic interactions are significant, the corrections in higher orders are not straightforward because of the complex cell-size dependences of formation energies.[29,30] We tested the Makov-Payne method for selected native defects in $NaTaO_3$ and will discuss the results in Sec. II C.

B. Computational details

The first-principles calculations were performed by the projector augmented-wave (PAW) (Ref. 31) method as implemented in the Vienna *ab initio* simulation package (VASP) (Refs. 32–34). The exchange-correlation functional is constructed by the GGA proposed by Perdew, Burke, and Ernzerhof.[35] PAW data sets with radial cutoffs of 1.2, 1.5, 0.8, and 1.5 Å were used for Na, Ta, O, and La, respectively. To describe the electronic wave functions with a plane-wave basis set, an energy cutoff of 400 eV was employed.

In order to investigate the structural and electronic properties of the $NaTaO_3$ perfect crystal, we performed geometry optimization for the unit cell. The Brillouin zone was sampled using a $6\times6\times6$ k-point mesh generated on the

basis of the Monkhorst-Pack[36] scheme with the Γ point centered. The cubic phase ($Pm\bar{3}m$ with $a=b=c=3.929$ Å and $\alpha=\beta=\gamma=90°$) (Ref. 37) was considered in the present study; it is very close to the monoclinic phase ($P2/m$ with $a=3.8995$ Å, $b=3.8965$ Å, and $c=3.8995$ Å, $\alpha=\gamma=90°$, and $\beta=90.15$) (Ref. 38) that shows, according to recent reports,[39,40] the highest photocatalytic efficiency among various structures of $NaTaO_3$. As expected from the similarity in the lattice structures, the electronic structures of the cubic and monoclinic phases have been reported to be very similar.[39–42] The lattice constant of the cubic structure was computed to be 3.975 Å in the present work and is in good agreement with the experimental value of 3.929 Å (Ref. 37). The calculated electronic structure will be detailed in Sec. III A.

For the simulation of native defects and La impurities, we used a $3\times3\times3$ supercell containing 135 atoms. The Brillouin zone was sampled using a $2\times2\times2$ mesh with the Γ point centered. The atomic positions were relaxed until the Hellmann-Feynman force on each atom was reduced to within 0.02 eV/Å in all the calculations. Various native defects, i.e., the Na vacancy (V_{Na}), the Ta vacancy (V_{Ta}), the O vacancy (V_O), the Na antisite (Na_{Ta}), and the Ta antisite (Ta_{Na}), and La impurities at the Na site (La_{Na}) and Ta site (La_{Ta}), were examined. Interstitial defects and impurities are excluded here because the close-packed perovskite-type structure makes the formation unlikely.

Concerning the VBM correction, we obtained the average potential differences of up to 0.1 eV for all the defects in the relevant charge states. The resultant correction term, i.e., the average potential difference multiplied by the defect charge ranged only up to 0.5 eV for V_{Ta} and 0.2 eV for the other defects. The uncertainty of the VBM correction is not expected to affect the discussion given in Secs. II C and III C.

The band gap of the $3\times3\times3$ perfect-crystal supercell was calculated to be 2.27 eV using the total-energy differences (2.23 eV in one-electron structure). Therefore, we employed $\Delta E_g=1.83$ eV for the correction of the band gap and defect formation energies, which results in the corrected band gap being equal to an experimental value of 4.1 eV (Ref. 43). The correction of formation energies was applied to V_O and La_{Na} whose donor states are close to the CBM and the wave-function characteristics are similar to those of the CBM. For Ta_{Na}, a localized donor state was found to be induced slightly above the CBM, which will be described in Sec. III B. This state is mainly characterized by Ta $5d$ as well as the conduction band of perfect $NaTaO_3$. Therefore, we also applied the correction for Ta_{Na}. It is noted that the results before the band-gap correction can be readily recovered from Figs. 5 and 7 showing the Fermi-level dependence of the formation energies (presented later). When the correction is not applied, the range of the Fermi level is truncated at the calculated CBM ($E_F=2.27$ eV). Because all the donorlike defects exhibit the highest charge states without occupied in-gap states in the whole range of the Fermi level, the positions of the lines representing formation energies are preserved for all the defects.

C. Image charge interaction

The correction for image charge interactions using the Makov-Payne method was tested for the native defects in the highest charge state, i.e., V_{Na}^-, V_{Ta}^{5-}, Na_{Ta}^{4-}, Ta_{Na}^{4+}, and V_O^{2+}. The formation energies of these defects before and after the atomic relaxation were obtained using four kinds of supercells containing 40, 135, 320, and 625 atoms, respectively. For V_O, which exhibits an exceptional behavior as described below, the neutral and + charge states were also investigated. The results are presented in Fig. 2 as a function of L^{-1}, where L denotes interdefect distance equivalent to the cell constant. The values without the VBM alignment are shown because it can lead to the double count of the correction. In addition, the band-gap correction, which is to be applied to V_O^0 and V_O^+, has not been considered to compare raw values.

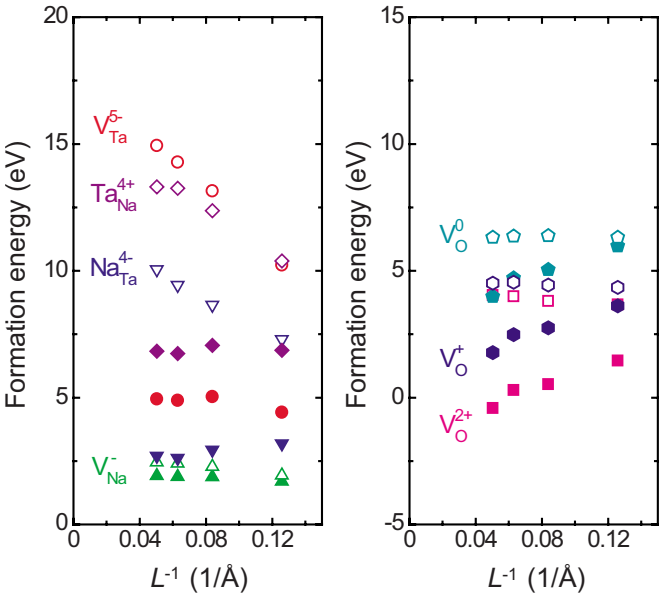

FIG. 2. (Color online) Formation energies of selected native defects as a function of L^{-1} (where L denotes interdefect distance). The energies are for $E_F=0$ and equilibrium condition 1 (O-rich limit). The band gap and VBM corrections are not included. The open and filled symbols denote the values before and after atomic relaxation, respectively.

In the case of V_{Na}^-, V_{Ta}^{5-}, and Na_{Ta}^{4-}, nearly linear L^{-1} dependences with negative slopes are recognized for the values before atomic relaxation. The slopes are close to those estimated using the formal defect charges and an experimental static dielectric constant indicating the dominance of the Madelung energy contributions. For Ta_{Na}^{4+}, the deviation from the linear dependence implies an overlap of higher-order terms. After relaxation, the cell-size dependences are markedly reduced for all of these defects as a result of an electronic relaxation concomitant with the atomic relaxation and/or the overlap of elastic effects.

The formation energies of V_O before atomic relaxation also show nearly linear dependences for all the charge states. As expected from the Madelung energy contribution, the neutral charge state has almost no cell-size dependence and the slope increases toward the negative side with the increase in the defect charge. The formation energies after relaxation significantly decrease as the cell size increases (L^{-1} decreases) and the cell-size dependences are similar to each other. This behavior of V_O after relaxation may be attributed to elastic effects, which was also found in the previous first-

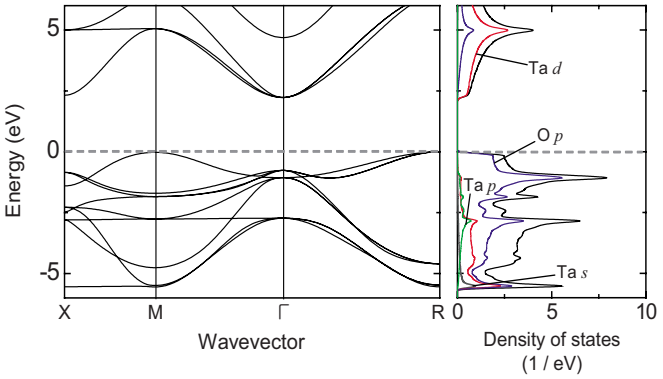

FIG. 3. (Color online) Band structure (left) and total and partial DOS (right) of the $NaTaO_3$ perfect crystal. The VBM is set at 0 eV as indicated by the dashed line. $X=(1/2,0,0)$, $M=(1/2,0,1/2)$, $\Gamma=(0,0,0)$, and $R=(1/2,1/2,1/2)$.

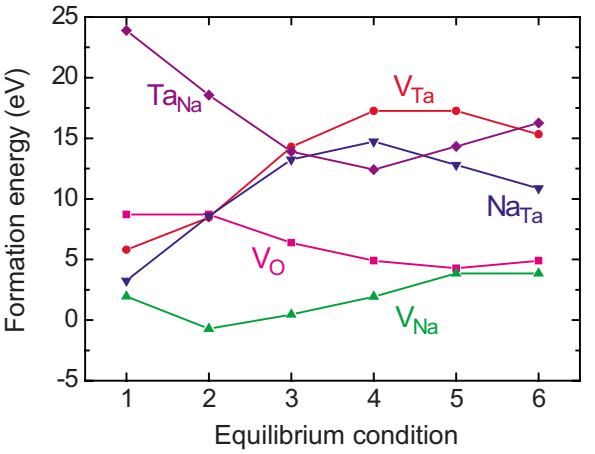

FIG. 4. (Color online) Formation energies of neutral native defects under six equilibrium conditions indicated in Fig. 1.

principles studies of V_O in perovskite $SrTiO_3$ (Refs. 44 and 45).

Summarizing these results, the cell-size dependences are small for the defects other than V_O after relaxation. When the 135-atom supercells are used, the formation energies are different by only up to 0.7 eV from those extrapolated to the dilute limit ($L^{-1}\rightarrow 0$) by assuming the L^{-1} and L^{-3} dependences. In other words, the corrections based on the Makov-Payne method (and the corrections for elastic contributions) cause changes of this amount. Thus, we estimate the errors of the formation energies to be less than 0.7 eV, which do not affect the relative defect energetics discussed later. For V_O, the strong elastic contribution after relaxation makes the extrapolation to the dilute limit difficult; whereas the dependence of the elastic contribution has been reported to be linear against L^{-1} (Ref. 29), the present results seem to deviate from it. A crude estimate assuming the L^{-1} dependence yielded values that are 2–3 eV lower than those for the 135-atom cells. However, even such 2–3 eV changes do not alter our discussion as shown later. In addition, similar dependences for the three charge states suggest that the transition levels are not significantly affected. In Sec. III we present the results without the corrections for electrostatic and elastic interactions, i.e., those from 135-atom cells with the VBM and band-gap corrections only for consistency.

III. RESULTS AND DISCUSSION

A. Electronic structure of perfect $NaTaO_3$

The electronic structure of the $NaTaO_3$ perfect crystal was studied as basic work for the investigation of native defects and impurities in this material. Figure 3 shows the calculated band structure and the total and partial density of states (DOS) of the perfect crystal with a five-atom unit cell. For the DOS, a Γ-centered $24\times24\times24$ k-point mesh was used for the Brillouin-zone integration and the eigenvalues were interpolated using a corrected tetrahedron method.[46]

As shown in Fig. 3, the band structure of perovskite-type cubic $NaTaO_3$ is calculated to be the indirect-gap type. The calculated gap is 2.23 eV, which is much smaller than the experimental value of ~4.1 eV (Ref. 43) owing to the well-known GGA shortcoming. The CBM is located at the Γ (0,0,0) point, while the VBM is located at the R (1/2,1/2,1/2) point. The state of the conduction-band edge at X (1/2,0,0) and that of the valence-band edge at M (1/2,0,1/2) have very similar energies to the CBM and VBM, respectively.

The valence-band ranges from −5.7 to 0 eV and is mainly characterized by O $2p$. The conduction band mainly consists of Ta $5d$. There is also a large component of O $2p$ in the conduction band mixed with Ta $5d$. Ta $6s$ and Ta $6p$ constitute the deep states in the valence band hybridizing with O $2p$. The states associated with Na $3s$ and $3p$ are found in a high-energy region in the conduction band and do not appear near the band gap. The overall features of our results are similar to those of previously reported computational results obtained by the full-potential-linearized-augmented-plane-wave (LAPW) (Ref. 41) and full-potential-linear muffin-tin-orbitals (LMTO) (Ref. 42) methods.

B. Vacancy and antisite defect in $NaTaO_3$

Figure 4 shows the formation energies of neutral defects V_O, V_{Na}, V_{Ta}, Na_{Ta}, and Ta_{Na} under each equilibrium condition. The formation energy of V_{Na} is relatively low, in particular, between conditions 1 and 3 (Na-poor and O-rich conditions). Under these conditions, the formation energy of V_O is relatively high and decreases toward O-poor conditions (conditions 4–6), while that of V_{Ta} is relatively low and increases toward the O-poor conditions. For antisite defects, namely, Na_{Ta} and Ta_{Na}, the formation energies are high under most equilibrium conditions. However, they are very sensitive to the equilibrium condition. The formation energy of Na_{Ta} under condition 1, for instance, is as low as that of V_{Na}. The formation energies of V_{Na} and V_{Ta} calculated here are similar to the reported values for cation vacancies in isostructural systems $NaNbO_3$ (Ref. 47) and $KTaO_3$ (Ref. 48).

To discuss the stability of defects, the Fermi-level dependence of the formation energies was investigated because the energetically favorable charge state of defects can vary with the Fermi level. Figure 5 shows the defect formation energies against the Fermi level in two extreme cases: condition 1 (O-rich limit) and condition 5 (O-poor limit). Under condi-

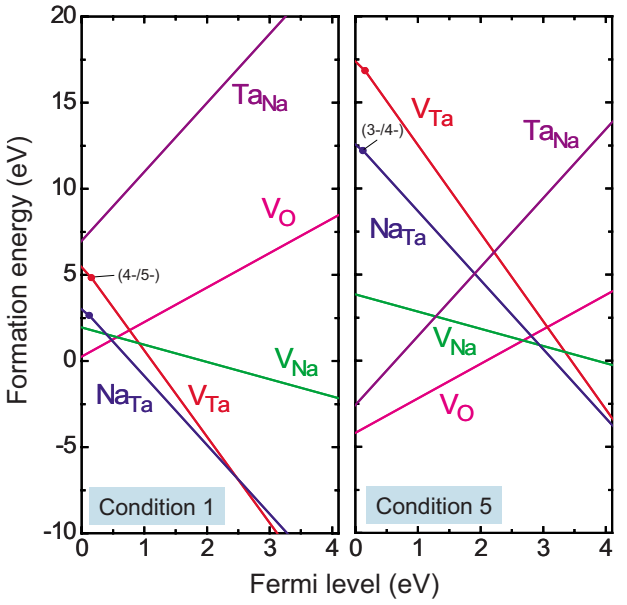

FIG. 5. (Color online) Formation energies of native defects as a function of the Fermi level under condition 1 (O-rich limit) and condition 5 (O-poor limit).

tion 1, Na_{Ta} and V_{Ta} have the lowest formation energies in a wide range of the Fermi level. The transition levels of Na_{Ta} and V_{Ta} are close to the VBM, $\varepsilon(3-/4-)=0.1$ eV for Na_{Ta} and $\varepsilon(4-/5-)=0.2$ eV for V_{Ta}, while other levels are not found in the band gap. Therefore, these are shallow acceptors. Their formation energies are negative when $E_F > 0.8$ eV for Na_{Ta} and >1.1 eV for V_{Ta}, resulting in spontaneous formation. Since these defects are expected to provide up to four holes per Na_{Ta} and five holes per V_{Ta}, E_F will be pushed down below 0.8 eV. As a result, n-type $NaTaO_3$ is not preferable under O-rich conditions. On the other hand, Ta_{Na} has a very high formation energy and is hence quite unstable.

Under condition 5, the formation energy of V_O is very low (and can be further lowered by 2–3 eV owing to the strong elastic effects mentioned in Sec. II C). It shows only the 2 + charge state throughout the whole range of the Fermi level. V_O is therefore a double donor that provides two electrons and its concentration can be high. Ta_{Na}, a quadruple donor, also shows good stability in the p-type region, i.e., when E_F is close to the VBM. In the n-type region, the formation energies of the two acceptorlike defects, Na_{Ta} and V_{Ta}, are negative when $E_F > 3.2$ eV for Na_{Ta} and >3.4 eV for V_{Ta}. The other acceptorlike defect V_{Na} is also likely to form. As a result, carrier electrons will be compensated by the holes released from these acceptors indicating that it is difficult to grow highly n-type $NaTaO_3$.

Figure 6 shows the site-decomposed DOS in the vicinity of the native defects in the highest charge states. For all the defects, localized states are not found in the calculated band gap. This means that the defect charges are not strong enough to hold free electrons or holes locally on their sites. Instead V_{Ta}^{5-} and Na_{Ta}^{4-} introduce deep localized states at ~16 eV below the VBM, which are characterized by their nonbonding O neighbors. The valence O $2p$ components of

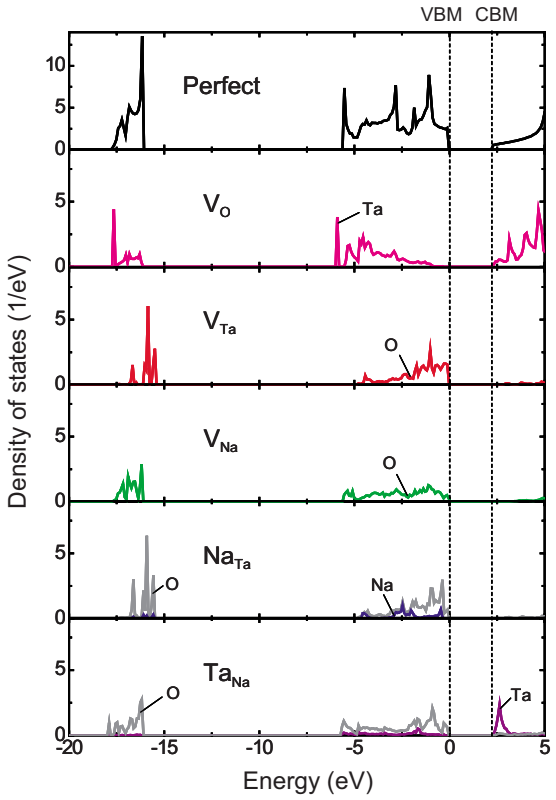

FIG. 6. (Color online) Site-decomposed electron DOS in the vicinity of V_{Na}^{-}, V_{Ta}^{5-}, V_O^{2+}, Na_{Ta}^{4-}, and Ta_{Na}^{4+} (per atom) along with the total DOS of the perfect crystal (per unit cell). The solid curve denotes the DOS of the defect-related atoms. The DOS of the Na component of Na_{Ta}^{4-} and the Ta component of Ta_{Na}^{4+} are, respectively, multiplied and divided by five for easy visualization. The dashed lines indicate the positions of the CBM and VBM.

both defects are very similar, which means that Na of Na_{Ta}^{4-} does not strongly couple to the nearby two O atoms. For Ta_{Na}^{4+}, the calculated electronic structure is quite different from that of V_{Na}^{-}. Slightly above the CBM, an unoccupied localized state is induced by the antisite Ta $5d$ hybridized with nearby twelve O $2p$. For the other charge states, we found that the localized state is partially occupied by electrons. However, this does not produce any in-gap state.

The distances between the native defects and their nearest neighboring atoms are summarized in Table I. The neighboring atoms of V_{Na}, V_{Ta}, V_O, and Na_{Ta} are displaced outward, whereas those of Ta_{Na} are displaced inward. Except for Ta_{Na}, there is almost no dependence on the charge state—indicating a weak dependence of the electronic structure on the charge state. This is consistent with the behavior of these defects as shallow donors or shallow acceptors suggested from the transition levels and the one-electron structures. For Ta_{Na}, the occupancy of the localized state changes the interaction with the neighboring atoms.

C. Lanthanum impurity in $NaTaO_3$

In order to elucidate the role of La impurities, we examined the formation energy of substitutional La as a function of the atomic chemical potentials and the Fermi level. As

TABLE I. Distances between defects and their nearest neighboring atoms after atomic relaxation. X (perfect) (X=Na, Ta, and O) denotes the distance between atom X and its neighbors in the perfect crystal. The neighboring atomic species and their coordination numbers are shown in parentheses.

Defect	Distance (Å)	Defect	Distance (Å)
Na (perfect)	2.811(O×12)	Na (perfect)	2.811(O×12)
V_{Na}^{0}	2.867	Ta_{Na}^{0}	2.606
V_{Na}^{-}	2.872	Ta_{Na}^{+}	2.594
Ta (perfect)	1.988 (O×6)	Ta_{Na}^{2+}	2.573
V_{Ta}^{0}	2.099	Ta_{Na}^{3+}	2.540
V_{Ta}^{-}	2.100	Ta_{Na}^{4+}	2.519
V_{Ta}^{2-}	2.101	Ta (perfect)	1.988 (O×6)
V_{Ta}^{3-}	2.101	Na_{Ta}^{0}	2.111
V_{Ta}^{4-}	2.105	Na_{Ta}^{-}	2.111
V_{Ta}^{5-}	2.111	Na_{Ta}^{2-}	2.111
O (perfect)	1.988 (Ta×2)	Na_{Ta}^{3-}	2.111
V_{O}^{0}	2.082	Na_{Ta}^{4-}	2.112
V_{O}^{+}	2.085		
V_{O}^{2+}	2.087		

positions of the doped La, we considered two substitutional sites, La_{Na} and La_{Ta}. Because the ionic radius of La^{3+} (1.34 Å) (Ref. 49) is as large as that of Na^{+} (1.39 Å) (Ref. 49), the location of La at the interstitial site is also unlikely because of the close-packed structure.

Figure 7 shows the calculated formation energies of La_{Na} and La_{Ta}. For the neutral charge state, both La_{Na} and La_{Ta} have high formation energies under O-rich conditions (1 and 2). Going toward O-poorer conditions (3–6), the formation energy of La_{Na} is significantly lowered, whereas the formation energy of La_{Ta} increases and becomes much higher than that of La_{Na}. Only under condition 1, namely, at the O-rich limit, La_{Ta} is more stable than La_{Na}. However, the formation energy of La_{Ta} is still too high to form in a substantial concentration.

The formation energies of La_{Na} and La_{Ta} against the Fermi level are shown in Fig. 7(b) for the two extreme cases, namely, conditions 1 and 5 corresponding to the O-rich and O-poor limits, respectively. For La_{Na}, no transition level is found and the 2+ charge state is energetically favorable for the whole range of the Fermi level. On the other hand, La_{Ta} shows two transition levels near the VBM: $\varepsilon(0/-)=0.1$ eV and $\varepsilon(-/2-)=0.2$ eV. Therefore, La_{Na} and La_{Ta} are a shallow donor and shallow acceptor, respectively. Under O-rich conditions such as condition 1, it is expected that the growth of n-type $NaTaO_3$:La is difficult since La_{Ta} as well as native multiple acceptors (Na_{Ta} and V_{Ta}) are expected to form spontaneously and then compensate carrier electrons. Under O-poor conditions, La_{Ta} is more stable than La_{Na} only in a highly n-type region and has a positive formation energy throughout the whole range of the Fermi level. Thus, La_{Na} can induce a high electron concentration in $NaTaO_3$:La.

From the analysis of the one-electron structure, we found that both La_{Na} and La_{Ta} introduce no localized states in the calculated band gap. The site-decomposed electron DOS in

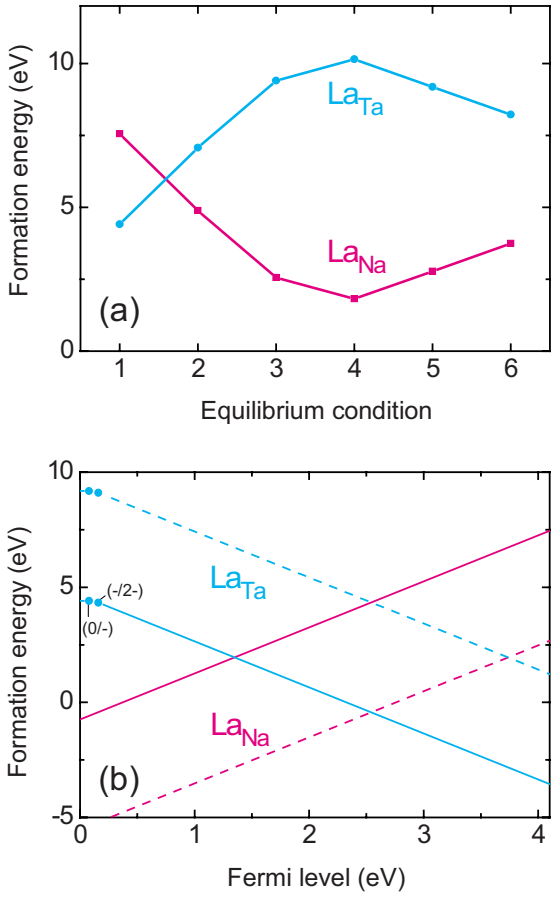

FIG. 7. (Color online) Formation energies of La_{Na} (pink) and La_{Ta} (cyan) (a) under six equilibrium conditions indicated in Fig. 1 and (b) as a function of the Fermi level under equilibrium condition 1 (solid) and condition 5 (dashed). For (a) only neutral charge states are shown.

the vicinity of La_{Na}^{2+} and La_{Ta}^{2-} is shown in Fig. 8. A notable feature of these DOS is the deep defect state of La_{Ta}^{2-} located at ~11 eV below the VBM. This state results from the coupling of La 5p, O 2s, and O 2p. Unlike the La_{Ta}^{2-}, no high DOS peak of La is found for La_{Na}^{2+}. The one-electron structures without localized states in the band gap for La_{Na} and La_{Ta} are consistent with the shallow donor/acceptor characteristics suggested from the transition levels shown in Fig. 7(b).

The atomic structures around La_{Na} and La_{Ta} are slightly relaxed, which are recognized in Table II. The neighboring O atoms of La_{Na} are displaced inward by 0.1 Å from their positions in perfect $NaTaO_3$, whereas the neighboring O atoms of La_{Ta} are displaced outward by 0.2 Å. The charge state dependence is very weak for both La_{Na} and La_{Ta}. Such different atomic displacements can be related to the difference in ionic radii. The ionic radii of 12-fold coordinated La^{3+} (1.36 Å) and Na^{+} (1.39 Å) (Ref. 49) are nearly the same, whereas those of sixfold-coordinated La^{3+} (1.03 Å) and Ta^{5+} (0.64 Å) (Ref. 49) are considerably different. The larger relaxation and high formation energy of La_{Ta} can be partly attributed to the large size mismatch.

On the basis of the experiments, the photocatalytic efficiency of $NaTaO_3$:La has been reported to become higher as

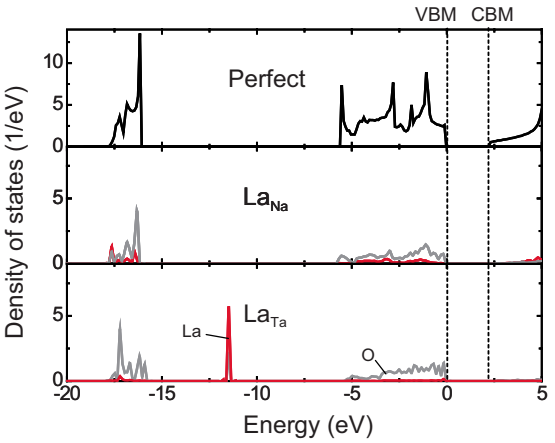

FIG. 8. (Color online) Site-decomposed electron DOS in the vicinity of La_{Na}^{2+} and La_{Ta}^{2-} (per atom) along with the total DOS of the perfect crystal (per unit cell). The red (darker) and gray (lighter) curves are, respectively, the DOS of the La and its neighbors in the defective supercell. For La_{Ta}, the DOS of La is divided by ten. The dashed lines indicate the positions of the CBM and VBM.

the La-doping level increases.[11] The formation of La_{Na} was suggested as a possible reason behind this high efficiency, which was expected to induce *n*-type conductivity, high crystallinity, and small crystal size.[11] However, the photocatalytic activity was decreased above some doping level and the suggested role of La_{Na} could not explain this opposite phenomenon.[11] Our results can be a guide for understanding such observed behavior of $NaTaO_3$:La. Under O-poor conditions (for instance, conditions 3–6), the intersection between the lines representing the formation energies of La_{Na} and La_{Ta} is located in an *n*-type region as recognized for condition 5 in Fig. 7(b). With a low La concentration, La should favor La_{Na} as a double donor, which is consistent with the suggestion in Ref. 11. However, such a formation of La_{Na} leads to the shift of E_F toward the CBM. As a result, after a certain La-doping level, La_{Ta} becomes more stable than La_{Na} and native multiple acceptors (V_{Ta} and Na_{Ta}) can also form, leading to the saturation in carrier concentration. The decrease in the photocatalytic activity experimentally observed for heavily La-doped $NaTaO_3$ might be attributed to the saturation in carrier concentration and the increase in the concentrations of La and the native acceptorlike defects that can act as recombination centers.

TABLE II. Distances between La and its nearest neighbors after atomic relaxation.

Impurity	Distance (Å)	Impurity	Distance (Å)
Na (perfect)	2.811(O×12)	Ta (perfect)	1.988(O×6)
La_{Na}^{0}	2.725	La_{Ta}^{0}	2.192
La_{Na}^{+}	2.722	La_{Ta}^{-}	2.192
La_{Na}^{2+}	2.720	La_{Ta}^{2-}	2.198

IV. SUMMARY

Using first-principles calculations, we investigated the formation energies and electronic structure of native defects and lanthanum impurities in $NaTaO_3$. Under O-rich conditions, the formation energies of Na_{Ta} and V_{Ta} are the lowest and negative throughout a wide range of the Fermi level. Under O-poor conditions, V_O is a dominant defect and acts as a double donor. Ta_{Na} has a high formation energy under most equilibrium conditions and it is expected to form only in a *p*-type region under O-poor conditions. In La-doped $NaTaO_3$, La_{Ta} is likely to form as a shallow acceptor under O-rich conditions whereas La_{Na} forms as a double donor under O-poor conditions. The site preference of La, however, also depends on the Fermi level, leading to self-compensation in heavily doped cases. In the one-electron structure, no localized defect state is found in the calculated band gap for all the considered defects. These electronic structures are consistent with the shallow donor or acceptor behavior suggested from the transition levels.

ACKNOWLEDGMENTS

This work was supported by three programs from the Ministry of Education, Culture, Sports, Science and Technology of Japan, i.e., Grants-in-Aid for Scientific Research (A), Priority Area on “atomic scale modification” (No. 474), and the global COE program.

*oba@cms.mtl.kyoto-u.ac.jp

[1] A. Kudo, Int. J. Hydrogen Energy **31**, 197 (2006).
[2] K. Yamaguti and S. Sato, J. Chem. Soc., Faraday Trans. 1 **81**, 1237 (1985).
[3] A. Kudo, K. Domen, K. Maruya, and T. Onishi, Chem. Phys. Lett. **133**, 517 (1987).
[4] K. Sayama and H. Arakawa, J. Chem. Soc., Faraday Trans. **93**, 1647 (1997).
[5] J.-M. Lehn, J.-P. Sauvage, and R. Ziessel, Nouv. J. Chim. **4**, 623 (1980).
[6] K. Domen, A. Kudo, T. Onishi, N. Kosugi, and H. Kuroda, J. Phys. Chem. **90**, 292 (1986).
[7] A. Kudo, K. Sayama, A. Tanaka, K. Asakura, K. Domen, K. Maruya, and T. Onishi, J. Catal. **120**, 337 (1989).
[8] H. G. Kim, D. W. Hwang, J. Kim, Y. G. Kim, and J. S. Lee, Chem. Commun. (Cambridge) **1999**, 1077.
[9] A. Kudo, H. Kato, and S. Nakagawa, J. Phys. Chem. B **104**, 571 (2000).
[10] K. Sayama and H. Arakawa, J. Photochem. Photobiol., A **77**, 243 (1994).
[11] H. Kato, K. Asakura, and A. Kudo, J. Am. Chem. Soc. **125**, 3082 (2003).
[12] A. Yamakata, T. Ishibashi, H. Kato, A. Kudo, and H. Onishi, J. Phys. Chem. B **107**, 14383 (2003).

[13] D. G. Porob and P. A. Maggard, J. Solid State Chem. **179**, 1727 (2006).
[14] Y. Lee, T. Watanabe, T. Takata, M. Hara, M. Yoshimura, and K. Domen, Bull. Chem. Soc. Jpn. **80**, 423 (2007).
[15] R. Asahi, T. Morikawa, T. Ohwaki, K. Aoki, and Y. Taga, Science **293**, 269 (2001).
[16] S. Na–Phattalung, M. F. Smith, K. Kim, M.-H. Du, S.-H. Wei, S. B. Zhang, and S. Limpijumnong, Phys. Rev. B **73**, 125205 (2006).
[17] M. Ni, M. K. H. Leung, D. Y. C. Leung, and K. Sumathy, Renewable Sustainable Energy Rev. **11**, 401 (2007).
[18] C. G. Van de Walle and J. Neugebauer, J. Appl. Phys. **95**, 3851 (2004).
[19] C. G. Van de Walle and R. M. Martin, Phys. Rev. B **35**, 8154 (1987).
[20] S. Pöykkö, M. J. Puska, and R. M. Nieminen, Phys. Rev. B **53**, 3813 (1996).
[21] T. Mattila and A. Zunger, Phys. Rev. B **58**, 1367 (1998).
[22] K. Matsunaga, T. Tanaka, T. Yamamoto, and Y. Ikuhara, Phys. Rev. B **68**, 085110 (2003).
[23] A. Togo, F. Oba, I. Tanaka, and K. Tatsumi, Phys. Rev. B **74**, 195128 (2006).
[24] S. B. Zhang, S. H. Wei, A. Zunger, and H. Katayama–Yoshida, Phys. Rev. B **57**, 9642 (1998).
[25] G. Makov and M. C. Payne, Phys. Rev. B **51**, 4014 (1995).
[26] M. Leslie and M. J. Gillan, J. Phys. C **18**, 973 (1985).
[27] J. Shim, E. K. Lee, Y. J. Lee, and R. M. Nieminen, Phys. Rev. B **71**, 035206 (2005).
[28] F. Oba, A. Togo, I. Tanaka, J. Paier, and G. Kresse, Phys. Rev. B **77**, 245202 (2008).
[29] C. W. M. Castleton, A. Höglund, and S. Mirbt, Phys. Rev. B **73**, 035215 (2006).
[30] C. W. M. Castleton and S. Mirbt, Phys. Rev. B **70**, 195202 (2004).
[31] P. E. Blöchl, Phys. Rev. B **50**, 17953 (1994).
[32] G. Kresse and J. Hafner, Phys. Rev. B **48**, 13115 (1993).
[33] G. Kresse and J. Furthmüller, Phys. Rev. B **54**, 11169 (1996).
[34] G. Kresse and D. Joubert, Phys. Rev. B **59**, 1758 (1999).
[35] J. P. Perdew, K. Burke, and M. Ernzerhof, Phys. Rev. Lett. **77**, 3865 (1996).
[36] H. Monkhorst and J. Pack, Phys. Rev. B **13**, 5188 (1976).
[37] International Center for Diffraction Data, JCPDS Card No. 74-2488, 2001.
[38] International Center for Diffraction Data, JCPDS Card No. 74-2479, 2001.
[39] W. H. Lin, C. Cheng, C. C. Hu, and H. Teng, Appl. Phys. Lett. **89**, 211904 (2006).
[40] C. C. Hu and H. Teng, Appl. Catal., A **331**, 44 (2007).
[41] Y. X. Wang, W. L. Zhong, C. L. Wang, and P. L. Zhang, Solid State Commun. **120**, 137 (2001).
[42] Z. H. Li, G. Chen, and J. W. Liu, Solid State Commun. **143**, 295 (2007).
[43] An experimental value of the monoclinic phase whose electronic structure is reported to be very close to that of the cubic phase in Ref. 39.
[44] J. P. Buban, H. Iddir, and S. Öğüt, Phys. Rev. B **69**, 180102(R) (2004).
[45] J. Carrasco, F. Illas, N. Lopez, E. A. Kotomin, Yu. F. Zhukovskii, R. A. Evarestov, Y. A. Mastrikov, S. Piskunov, and J. Maier, Phys. Rev. B **73**, 064106 (2006).
[46] P. E. Blöchl, O. Jepsen, and O. K. Andersen, Phys. Rev. B **49**, 16223 (1994).
[47] A. Shigemi and T. Wada, Jpn. J. Appl. Phys., Part 1 **43**, 6793 (2004).
[48] A. Shigemi, T. Koyama, and T. Wada, Phys. Status Solidi C **3**, 2862 (2006).
[49] R. D. Shannon, Acta Crystallogr., Sect. A: Cryst. Phys., Diffr., Theor. Gen. Crystallogr. **32**, 751 (1976).